Fast Feedback Control of Mechanical Motion Using Circuit Optomechanics

Cheng Wang, Louise Banniard, Laure Mercier de Lépinay, and Mika A. Sillanpää[*]

QTF Centre of Excellence, Department of Applied Physics, Aalto University, FI-00076 Aalto, Finland

Measurement-based control, using an active-feedback loop, is a standard tool in technology. Feedback control is also emerging as a useful and fundamental tool in quantum technology and in related fundamental studies, where it can be used to prepare and stabilize pure quantum states in various quantum systems. Feedback cooling of center-of-mass micromechanical oscillators, which typically exhibit high thermal noise far above the quantum regime, has been particularly actively studied and has recently been shown to allow ground-state cooling by means of optical measurements. Here we realize measurement-based feedback operations in an electromechanical system, cooling the mechanical thermal noise down to three quanta, limited by added amplifier noise. We also obtain significant cooling when the system is pumped at the blue optomechanical sideband, where the system is unstable without feedback.

I. INTRODUCTION

In cavity optomechanics, quantum control of mechanical motion can be achieved via radiation-pressure force from an optical light field on a mechanical degree of freedom in two different ways. Coherent quantum control involves applying a coherent pump tone to induce a strong coupling between the motion and an effective cold bath, so that the combined system evolves to a desired state. In measurement-based feedback control, an error signal obtained from a measurement result is applied as a force on the mechanical oscillator through a time-delayed and carefully filtered feedback loop to steer and control the evolution of motional states.

Feedback control and its ability to achieve cooling of massive mechanical objects has been investigated both theoretically and experimentally. It was first demonstrated in optics [1], with active experimental research following along the same lines [2–11]. Recently, feedback cooling down to the ground state was achieved for an ultrahigh-quality-factor SiN membrane resonator [12]. Feedback cooling also allowed the bringing of a 10-kg mass in the Advanced LIGO gravitational-wave detector close to its motional ground state [13,14]. Besides massive oscillators, levitated nanoparticles have been successfully feedback-cooled [15–19], some recent experiments even reaching the motional ground state [20,21].

Feedback control applied to a microwave optomechanical system [22,23] has yet to be realized. The implementation poses experimental challenges, but also has potential for operation deep in the quantum regime for which electromechanical systems are generally well suited. Typical microfabricated electromechanical resonators have rather high frequencies (greater than 5 MHz), which sets constraints for a digital realization of a control system, as high processing rates are required. Furthermore, since the electromagnetic degree of freedom has to react fast to the control, a microwave cavity with a high external coupling is necessary. This poses further challenges, as large external couplings are not easily combined with mechanical elements directly integrated in superconducting on-chip cavities. Here we realize feedback control in an electromechanical system with a drum mechanical membrane using a scheme adapted for this system, where we use a coherent tone to perform a strong measurement and a modulated tone to apply the adequate feedback force on the system.

II. THEORY

In measurement-based feedback cooling of a mechanical oscillator, the motion is continuously monitored with very high precision, which allows one to determine the oscillator's speed. A force proportional to the speed, which therefore acts as a viscous force, is fed back to the oscillator. This force artificially damps the motion without adding the fluctuation counterpart usually linked to damping mechanisms. This reduces the displacement variance, so the oscillator is effectively cooled. To cool the oscillator's thermal occupation number near the quantum ground state, it is critical that the measurement is close to the quantum-limited sensitivity. Indeed, measurement noise higher than the level of position quantum fluctuations results in feedback-force noise limiting the cooling efficiency above the quantum ground state.

---
[*]Mika.Sillanpaa@aalto.fi

A. Basic principle of feedback cooling

The principle of feedback cooling of mechanical oscillations is fairly well known [24–29] and is recalled here only briefly. The position x (for the moment given in meters) of an oscillator of mass M, frequency ω_m, and damping rate γ follows the evolution equation

$$\ddot{x}(t) = -\omega_m^2 x(t) - \gamma \dot{x}(t) + F_{\text{th}}(t)/M, \qquad (1)$$

where $F_{\text{th}}(t)$ is the Langevin force whose spectrum $S_F[\omega]$ in the classical limit is $S_F^{th}[\omega] = 2k_B T M \gamma$, with T the temperature of the oscillator's bath and k_B the Boltzmann constant. The spectrum of the position of the free oscillator is given by

$$S_x[\omega] = \frac{2k_B T \gamma}{M[(\omega_m^2 - \omega^2)^2 + \gamma^2 \omega^2]}. \qquad (2)$$

The damping rate appears both in the intensity of the coupling to the thermal bath and as the bandwidth of the Lorentzian mechanical spectrum. Application of a damping feedback force F_{FB} of $-gM\gamma\dot{x}$, where g is the feedback gain, broadens the spectrum $\gamma \to \gamma(1+g)$, resulting in

$$S_x[\omega] = \frac{2k_B T \gamma}{M[(\omega_m^2 - \omega^2)^2 + \gamma^2(1+g)^2\omega^2]}, \qquad (3)$$

which holds in the high-temperature limit, where quantum fluctuations can be ignored. This process of damping the oscillator without adding fluctuations has been coined "cold damping." Effectively, the resulting spectrum is that of an oscillator of damping $\gamma(1+g)$ at a temperature $T/(1+g)$, lower than the temperature of the bath T. This effect is therefore also called "feedback cooling." The process requires a measurement and a reaction to the measurement result much faster than the decay time of the oscillator $1/\gamma$. The cooling efficiency is limited by the amount of noise added in the feedback loop. This noise predominantly comes from the background noise in the detection of the oscillator's position.

B. Microwave optomechanical detection

We consider an archetypal optomechanical system, where a single mechanical harmonic mode (frequency ω_m and damping rate γ) is coupled to an electromagnetic cavity (frequency ω_c and damping rate κ). We ignore internal losses of the cavity. The cavity is probed by a strong coherent field (frequency ω_p), which is detuned from ω_c by an amount $\Delta = \omega_p - \omega_c$. The probing induces an effective optomechanical coupling $G = g_0\sqrt{n_c}$, where n_c is the number of photons driven in the cavity by the tone and g_0 is the vacuum optomechanical coupling.

To describe the feedback process, we treat the system using the standard input-output theory of optical cavities.

From now on, we treat the mechanical oscillator with dimensionless position $x(t)$ and momentum $p(t)$. We also define the dimensionless quadratures of the field in the cavity, $x_c(t)$ and $y_c(t)$ in the frame rotating at the cavity frequency. The equations of motion in the frequency domain are

$$\chi_c^{-1} x_c = -\Delta y_c + \sqrt{\kappa} x_{c,\text{in}},$$
$$\chi_c^{-1} y_c = \Delta x_c - 2Gx + \sqrt{\kappa} y_{c,\text{in}},$$
$$-i\omega x = \omega_m p,$$
$$(\gamma - i\omega)p = -\omega_m x - 2Gx_c + \frac{f_{\text{th}}}{\omega_m} + \frac{f_{\text{FB}}}{\omega_m}, \qquad (4)$$

where the cavity susceptibility is $\chi_c^{-1} = \kappa/2 - i\omega$, $x_{c,\text{in}}$ and $y_{c,\text{in}}$ are the input noise operators for the cavity, and f_{th} and f_{FB} are scaled forces: $f_X = \omega_m F_X/Mx_{\text{ZPF}}$, where F_X is a force, M is the effective mass, and x_{ZPF} is the zero-point fluctuation of the oscillator.

The feedback force f_{FB} is now present in addition to the thermal force. If information on the measured observable, position x, is contained in the feedback force, a closed feedback loop is formed.

In a generic optomechanical measurement, the output field

$$y_{\text{out}} = \sqrt{\kappa} y_c - y_{c,\text{in}} \qquad (5)$$

emitted from the cavity carries information about x. The nature of the feedback force is designed by one applying a suitable processing, or filter function, to the measured y_{out}. In a real situation, the measurement can provide only an approximation of x. This is primarily because a significant amount of noise is added to y_{out} before it is converted into a force. In microwave experiments, this noise, denoted as a random field $y_{\text{add}}(t)$, is due to transistor amplifiers. Even in the best cases, this noise is at least an order of magnitude higher than the quantum limit. The amplifier noise is typically characterized as the added number of noise quanta $\langle y_{\text{add}}[\omega] y_{\text{add}}[-\omega]\rangle = n_{\text{add}}$.

The feedback force is obtained by application of a filter function $A[\omega]$ to the signal, including a gain, and is scaled for convenience by $\sqrt{\kappa}$:

$$f_{\text{FB}}[\omega] = \frac{A[\omega]}{\sqrt{\kappa}} (y_{\text{out}}[\omega] + y_{\text{add}}[\omega]). \qquad (6)$$

To approximate a force proportional to the oscillator's velocity, we take the filter function $A[\omega]$ to be a phase-shifting (phase shift $\phi \in \mathbb{R}$) and amplifying (gain $A_0 > 0$) operation:

$$A[\omega] = A_0 \exp\left(-i\phi \frac{\omega}{\omega_m}\right). \qquad (7)$$

1. Resonant probing

The unresolved-sideband (bad-cavity) situation $\kappa \gg \omega_m$, where the cavity follows the mechanics without delay, allows a simple treatment of the entire process. Our experimental parameters, where $\kappa \approx \omega_m$, do not well satisfy this condition. The basic case of resonant probing ($\Delta = 0$), as shown in Fig. 1(a), allows some analytical results at arbitrary sideband resolution to be obtained (Appendix A). Here the effective susceptibility of the oscillator is similar to that implied by Eq. (3):

$$\chi_{\text{FB}}[\omega] = \frac{1}{-i\omega\gamma_{\text{eff}} + \omega_{\text{eff}}^2 - \omega^2}. \quad (8)$$

Here, for large mechanical quality factors $\omega_m/\gamma \gg 1$ (in the experiment $\omega_m/\gamma \sim 10^5$), the effective mechanical frequency and damping rate are, respectively,

$$\omega_{\text{eff}} \simeq \omega_m + \frac{2GA_0\left(\kappa\cos\phi + 2\omega_m\sin\phi\right)}{\kappa^2 + 4\omega_m^2}, \quad (9a)$$

$$\gamma_{\text{eff}} \simeq \gamma + \frac{4GA_0(\kappa\sin\phi - 2\omega_m\cos\phi)}{\kappa^2 + 4\omega_m^2}. \quad (9b)$$

At the optimum feedback phase satisfying

$$\phi_m = \tan^{-1}\left(-\frac{\kappa}{2\omega_m}\right) + \pi, \quad (10)$$

the resonant frequency is unchanged, and the damping is maximized, with the feedback-induced damping

$$\gamma_{\text{FB}} = \frac{4GA_0}{\sqrt{\kappa^2 + 4\omega_m^2}}. \quad (11)$$

The oscillator is supposed to couple to a bath with thermal occupation number n_m^T, which is usually much larger than 1. As mentioned earlier, the added feedback damping will induce cooling of the oscillator. However, there are competing processes that limit the cooling effect.

The mechanical noise energy is obtained from the spectral density of the oscillator's displacement, where we can identify three contributions. The thermal-plus-zero-point-fluctuation spectrum is cooled via the enhanced damping down to the variance:

$$n_T = \frac{\gamma}{\gamma_{\text{eff}}}\left(n_m^T + \frac{1}{2}\right). \quad (12)$$

As in generic optomechanical position measurements, the quantum backaction of the measurement tends to heat up the oscillator linearly with the cooperativity, adding a mechanical population:

$$n_{\text{QBA}} = C_{\text{eff}}\frac{\kappa^2}{\kappa^2 + 4\omega_m^2}. \quad (13)$$

The cooperativity C_{eff} appearing in this quantum backaction noise is the cooperativity defined from the damped oscillator's parameters:

$$C_{\text{eff}} = \frac{4G^2}{\kappa\gamma_{\text{eff}}}. \quad (14)$$

The increased damping of the oscillator (reduced C_{eff}) thus makes the oscillator less susceptible to the quantum backaction, and the backaction contribution n_{QBA} is reduced with increasing feedback gain.

The background noise in the detection in typical microwave-optomechanical systems is dominated by the
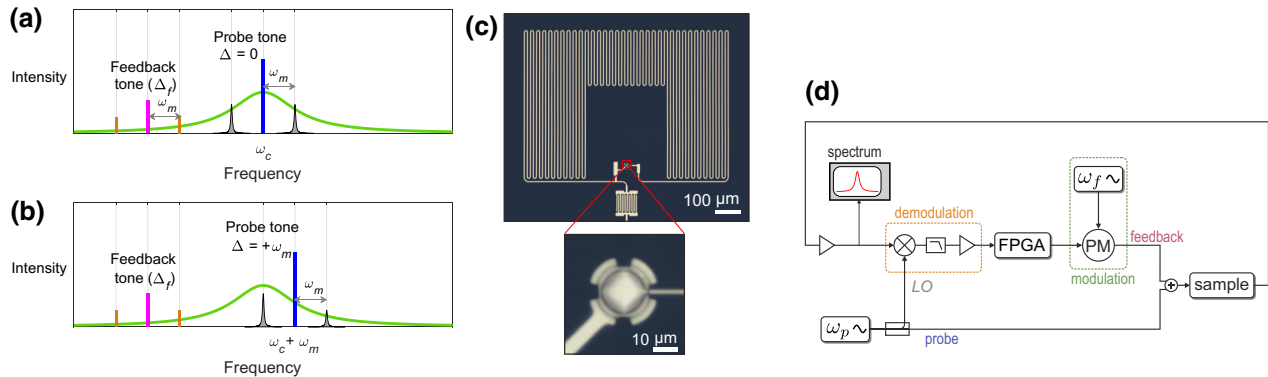

FIG. 1.   Feedback setup. (a) The basic frequency scheme of feedback cooling in cavity optomechanics, with the strong probe tone set at the cavity frequency ($\Delta = 0$). (b) The probe tone set alternatively to the blue mechanical sideband ($\Delta = \omega_m$). (c) Optical micrograph of a similar circuit-electromechanical device. The aluminum-drumhead oscillator of diameter 13 μm is connected to a meander inductor to form a cavity strongly coupled to a transmission line through a large external finger capacitor. An enlargement of the area of the drumhead is indicated by dashed red lines. (d) Simplified schematic of the microwave circuit around the electromechanical device; PM, phase modulator.

microwave-amplifier noise n_{add}. Here it is fed back to the oscillator, leading to additional mechanical fluctuations. Another, more-fundamental contribution is due to vacuum fluctuations associated with the measurement, which are also fed back to the mechanical oscillator. The sum of these is given as follows:

$$n_{FB} = \frac{A_0^2}{2\kappa \gamma_{eff}} \left(n_{add} + \frac{1}{2} \right). \qquad (15)$$

The total remaining mechanical occupation n_m under feedback cooling satisfies

$$n_m + \frac{1}{2} = n_T + n_{QBA} + n_{FB}, \qquad (16)$$

which decreases with increasing gain A_0 and then, for high gain, starts increasing again as n_{FB} becomes the dominant contribution to the occupation. The optimum cooling is reached when the oscillator is strongly damped, $n_T \ll 1$, and when the contributions of backaction and noise injection balance each other. This occurs when $G/A_0 = 1/4\sqrt{1 + 2n_{add}}\sqrt{\kappa^2 + 4\omega_m^2}/\kappa$, and results in the optimum cooling:

$$n_{m,min} + \frac{1}{2} = \frac{1}{2}\sqrt{1 + 2n_{add}}. \qquad (17)$$

To cool the system down to the ground state with $n_m < 1$, one has to reach $n_{add} < 4$. This is beyond reach of transistor amplifiers, but is possible with near-quantum-limited Josephson parametric amplifiers.

We now discuss the detection aspect. Under resonant probing of the cavity, the quadrature of the cavity output $y_{out} = i(a_{out}^\dagger - a_{out})/\sqrt{2}$, where a_{out} is the output-field annihilation operator, displays a mechanical signature at the optomechanical sidebands around the probe tone. In the experiment, the signal used to establish the feedback loop is the demodulated signal coming out of the cavity. For the data analysis, we also record the heterodyne spectrum

$$S_{out}[\omega] = \langle a_{out}^\dagger[\omega] a_{out}[-\omega] \rangle + \frac{1}{2}. \qquad (18)$$

Inference of the state of the mechanical oscillator based on the in-loop spectrum is complicated by the fact that the injected noise and the reflected noise are out of phase, which leads to "noise squashing," or destructive interference close to the mechanical resonance. This becomes relevant at strong feedback strength around the optimum cooling; see Eq. (17). In the bad-cavity case, one can easily identify correlations leading to the squashing; see Appendix B. In the case of arbitrary sideband resolution, we calculate the theoretical output spectra numerically (see Appendix A) from the solution of the equations of motion, Eq. (4), and from the input-noise correlators.

2. Blue-sideband probing

For optomechanical systems with $\kappa \lesssim \omega_m$, blue-sideband probing leads to optomechanical antidamping. The damping rate is reduced by

$$\gamma_{opt} = \frac{4G^2}{\kappa} \frac{1}{1 + \left(\frac{\kappa}{4\omega_m} \right)^2}. \qquad (19)$$

If this antidamping rate overcomes the intrinsic, or otherwise-enhanced, damping rate of the mechanical oscillator, the latter becomes unstable.

It has been shown that blue-sideband pumping can be used to drive a stable steady state, but only if combined with other processes that stabilize the system. Examples include optomechanical dissipative squeezing and entanglement [30–34], which count on steadying dynamical backaction effects dominating backaction noise in some regimes to allow the squeezing of a quadrature, in spite of a simultaneous increase of the effective bath temperature for that quadrature because of backaction noise.

A similar competition of effects exists in the present case: large probe powers provide large detection sensitivities beneficial to the feedback process, but also large optomechanical amplifications that can result in instability. The gain of the feedback loop can be chosen independently from the probe power, so a good configuration of feedback parameters is expected to produce cooling. The question is then whether the strong cold-damping effect obtained from this efficient measurement can, for some range of parameters, dominate optomechanical antidamping. We find that the answer is yes. The effective mechanical damping rate in the scheme in Fig. 1(b) is the sum of the rates due to dynamical backaction and the feedback cooling:

$$\gamma_{eff} = \gamma - \gamma_{opt} + \frac{4GA_0 \left[(\kappa^2 + 8\omega_m^2) \sin\phi - 2\kappa\omega_m \cos\phi \right]}{\kappa^3 + 16\kappa\omega_m^2}. \qquad (20)$$

Because the feedback has to first counteract the amplification induced by dynamical backaction, a larger gain as compared with the gain required for resonant probing is needed, which in turn will inject more noise and tend to reduce the cooling performance. Ground-state cooling is still possible, but very little added noise can be tolerated.

C. Feedback scheme

In some feedback-cooling experiments, a single laser is used both for probing and applying the feedback force by radiation pressure [7,11]. A situation described by Eq. (4) requires a separate method to create the force. One possibility is to use direct mechanical actuation [13]. Most

optomechanical experiments have used another laser dedicated to applying the feedback force. We adapt this technique in this work, and create the feedback force by suitable modulation of another microwave tone, a relatively weak feedback tone.

The basic frequency scheme is shown in Fig. 1(a), where the probe tone frequency is set at the resonance of the cavity. The feedback tone is typically detuned from the cavity by a detuning Δ_f larger than several cavity linewidths. This large frequency separation between microwave tones allows us to treat all optomechanical processes independently. Similar reasoning holds also for the other explored alternative, the blue-sideband probing shown in Fig. 1(b).

At room temperature, the cavity output field is homodyne-detected by demodulation with a local oscillator at the probe tone frequency ω_p, as seen in Fig. 1(d). The phase of the local oscillator (with respect to the phase of the driving tone) is tuned to measure the quadrature y_c carrying the most information on the mechanical oscillator. The demodulated quadrature is a direct record of the position, appearing as an oscillatory signal at frequency ω_m in the laboratory frame. This signal, once phase-shifted and amplified, is used to realize a weak phase modulation of a second microwave tone (the feedback tone) at frequency $\omega_f = \omega_c + \Delta_f$. This effectively generates a triplet of frequencies separated by ω_m, centered at ω_f. With an adequate setting for the feedback phase shift, the amplitude of each sideband of the driving triplet is approximately proportional to the velocity $\dot{x}$, while the central peak has a constant, much-larger amplitude. Each sideband interferes with the central peak to produce a feedback force linear in sideband amplitude (see Appendix C); that is, proportional to $\dot{x}$. Cross-products of sidebands generate a force dependent on the mechanical energy, which is maintained negligible in comparison with the linear feedback force by our keeping the amplitude of the central peak much larger than the amplitude of the sidebands. For details on generation of the feedback force, see Appendix C.

III. EXPERIMENTAL SETUP

A. Electromechanical device

A microwave optomechanical device is used in which an aluminum-drum oscillator is coupled to a superconducting microwave resonator (the cavity). Photographs of the device are shown in Fig. 1(c). The aluminum-drum oscillator is a parallel-plate capacitor with a vacuum gap, consisting of an aluminum membrane suspended above an aluminum electrode. It oscillates at frequency $\omega_m/2\pi = 8.14$ MHz and has intrinsic damping rate $\gamma/2\pi = 76$ Hz. An LC circuit formed by this plate capacitor and a meandering inductor sustains a resonance at microwave frequency $\omega_c/2\pi = 5.35$ GHz. The device structure and fabrication is otherwise standard [33,34], but

the microwave cavity is strongly coupled to a transmission line by means of a large interdigitated capacitor with capacitance of approximately 15.5 fF, on the same order as the drum capacitance. The cavity is overcoupled, with the total decay rate $\kappa/2\pi = 8.5$ MHz dominated by external coupling and containing a small contribution $\kappa_I/2\pi = 660$ kHz due to internal cavity losses.

The device is maintained at a somewhat elevated temperature of 80 mK, where $n_m^T \simeq 205$, in a dilution refrigerator. We chose an operating temperature clearly higher than the base temperature, because we observed intermittent "spiking" [35] of the mode temperature at lower temperatures.

The single-photon optomechanical coupling is $g_0/2\pi \simeq 130$ Hz. The calibration of the effective coupling G of the probing tone is realized by our monitoring the sideband-cooling effect as described in Appendix D. The values of the enhanced couplings of all tones used in this work are inferred from this calibration and from the measurement of the cavity susceptibility.

B. Feedback setup

The cavity output signal, Eq. (5), which mainly consists of the two optomechanical sidebands generated by the probe tone, is amplified inside the refrigerator with an amplifier exhibiting the effective noise $n_{\text{add}} \simeq 13$ quanta, and is then demodulated with use of the probe tone as a local oscillator to realize a homodyne detection. The demodulation result is passed through an analog bandpass filter (bandwidth of 5–11 MHz) to retain the signal oscillating at the mechanical frequency, while limiting unnecessary broadband noise before digitization. The signal is then sent to a 14-bit field-programmable-gate-array (FPGA)-backed acquisition device (Red Pitaya STEMlab 125-14) with an input and output sampling rate of 125 MHz. The FPGA card is programmed to replay this signal, after further digital bandpass filtering (1-MHz bandwidth), time delaying, and amplification [36].

Both the derivative and the phase-shifting feedback functions assume unlimited feedback bandwidth, so in this sense the mentioned bandpass filtering is not needed, and in principle it even limits the cooling. The reason for our implementing the bandpass filtering is to cut off unnecessary off-resonant noise that otherwise would saturate the amplification setup or that would lead to loss of the useful information in the digitization noise.

To cool all the relevant frequency components of the oscillator's motion, the passband width has to be much larger than γ_{eff}, which is satisfied in our case. It is not practical to further try to reduce the bandwidth, since it is technically very difficult if not impossible to produce a relatively flat passband response of, say, 1% bandwidth centered at ω_m.

The FPGA output signal is sent to a microwave phase modulator to modulate the feedback tone at frequency ω_f. This phase modulation, being very weak, is essentially comparable to an amplitude modulation, and generates mechanical-momentum-dependent sidebands $\pm\omega_m$ around a strong coherent peak at ω_f. The details are given in Appendix C.

Since the feedback tone (and its modulation sidebands) sits far on the red side of the cavity, the cavity suscepti-bility significantly shifts the phase of the feedback force, by an estimated 72°. The tunable contribution to the phase shift is eventually tuned to produce a total phase shift of $\phi_m + 2n\pi$ ($n \in \mathbb{N}$) between the position signal and the feedback force. As long as the total number of additional periods n by which the force is delayed from the momentum signal remains much smaller than the quality factor of the mechanical oscillator, the feedback performance is not significantly affected by this additional delay.

Both sidebands of the feedback triplet mix with the strong central coherent peak of the triplet, generating a term in the feedback force with a slightly different phase shift, as the cavity susceptibility and microwave transmission lines contribute differently to the total phase shift for each component of the driving triplet. These two contributions to the feedback force, containing versions of the mechanical signal phase-shifted by different amounts, do not necessarily add up fully constructively (see Appendix C), but one is sufficiently attenuated by the cavity suscep-tibility to limit the effect of a destructive interference and allow there to be a relatively strong feedback force in the experimental situation.

IV. RESULTS

A. Probing at the cavity frequency

The probe tone is first positioned at the cavity fre-quency ($\Delta \simeq 0$), such that the displacement spectrum of the oscillator is encoded in the cavity output spectrum with the maximum transduction efficiency while maintain-ing mechanical stability. In practice, we set Δ to negative values of a few kilohertz, which ensures the system is sta-bler toward a possible drift of the cavity frequency, while still having a negligible optically induced damping. The feedback tone is detuned by $\Delta_f/2\pi = -20$ MHz from the cavity frequency. This detuning is chosen such that $|\Delta_f| > 2\omega_m$ to avoid integration of stray-feedback-field components into the measurement of the position, but is kept on the order of κ to allow there to be a significant response of the cavity.

Next we vary the feedback phase ϕ and record the prop-erties of the mechanical peaks in the heterodyne spectrum. The peaks are primarily characterized by their frequency, Eq. (9a), and linewidth, Eq. (9b). We show the phase dependence of these quantities in Figs. 2(a) and 2(b). The data are not plotted in the regime where the system is unstable ($\gamma_{\text{eff}} < 0$). Aside from the effect of the feed-back, the mechanical frequency is expected to undergo a redshift under the strong probe driving due to the second-order optomechanical coupling. The shift is given by $\delta f_2 = -\frac{1}{2}g_2 n_c$, where $g_2 = \frac{1}{2}d^2\omega_c/dx^2 x_{\text{ZPF}}^2$. With the experimen-tal parameters, we expect $\delta f_2/2\pi \simeq 400$ Hz. However, the frequency at zero feedback gain is observed to be red-shifted by 1.2 kHz with respect to its value calibrated independently. We believe that the additional shift is due to occasional drifts of the intrinsic mechanical frequency observed during the cooldown. For the feedback-induced frequency shifts shown in Fig. 2(a), we thus use the zero value of the shift as a free parameter, common to all traces.

With this adjustment, we reach good agreement with the theoretical predictions, leaving a phase offset φ as another adjustable parameter. This offset is defined to contain the phase shifts due to transduction, as detailed in Appendix C, and an unknown contribution due to the time delays in the system. More specifically, in Eqs. (9a) and (9b), we
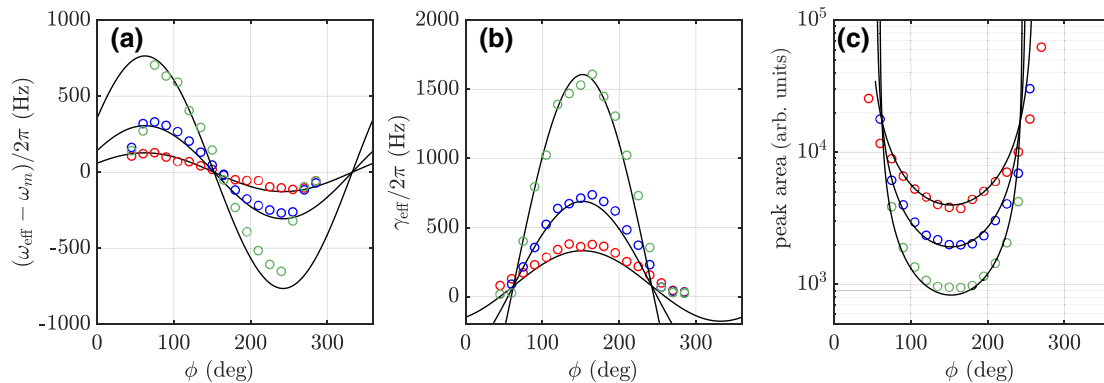

FIG. 2.　Feedback-control measurements. We use a strong probe tone at the cavity center frequency ($\Delta = 0$), with effective coupling $G/2\pi \simeq 420$ kHz. The data in each panel correspond to feedback gain $A_0/2\pi = 2.8$ kHz (red), $A_0/2\pi = 6.7$ kHz (blue), and $A_0/2\pi = 16.7$ kHz (green). The solid lines are theoretical fits. (a) Mechanical frequency shift and (b) effective damping rate as functions of feedback-loop phase. (c) Area of the mechanical peak in the heterodyne output spectrum.

identify $\phi \Rightarrow \phi + \varphi$ and use φ as an adjustable parameter when we fit Eqs. (9a) and (9b) to the data shown in Fig. 2. We also study the phase dependence of the area of the mechanical peaks as shown in Fig. 2(c). In the limit of weak feedback, where the noise squashing plays little role, the peak area is a good measure of the temperature of the mechanical mode. This condition is satisfied in the data shown in Fig. 2, where γ_{eff} reaches values up to approximately $2\pi \times 1$ kHz. A cooling by 1 order of magnitude is observed in Fig. 2(c), where the reference is the crossing point of the curves corresponding to zero cooling or amplification.

The maximum damping from the phase-sweeping measurements is determined at a phase value around $145° \pm 5°$, which according to Eqs. (9a) and (9b) corresponds to an optimized loop delay to exert a damping force proportional to the velocity. Notice that this phase differs from the optimum value $\phi_m = 90°$ expected in the bad-cavity limit. With this optimized phase, we proceed to vary the feedback gain up to large values and investigate the maximum cooling we can achieve.

We show in Figs. 3(a) and 3(b) the two peaks of the in-loop heterodyne spectra. At high gain, the peaks are not equal. The lower sideband of the probe tone exhibits less squashing than the upper sideband. This can be interpreted as a manifestation of the sideband asymmetry that has been studied in various optomechanical systems [37–39]; see Eq. (B1). For the theoretical fits, we use the bath temperature for each gain as the only adjustable parameter because we anticipate the mechanical bath may be heated up as the gain increases. We indeed observe a heating of the bath from $n_m^T \simeq 200$ to $n_m^T \simeq 370$ between zero and the high feedback-gain values (Fig. 5). Overall, the theory gives a good fit to the data. There is some discrepancy at the highest gain values in the upper sideband, which we speculate is due to noise related to the feedback tone

circulating in the system, the exact origin of which remains to be clarified.

According to Eq. (9b), the mechanical linewidth evolves linearly with respect to the feedback gain. We test this basic property as shown in Fig. 3(c). At high gain values, the peaks become distorted due to noise squashing, and these data are not considered in this situation. The solid line in Fig. 3(c) is a linear fit that is the basis for creating the theoretical spectra in Figs. 3(a) and 3(b), according to Eqs. (D4) and (D5). At zero gain, the linewidth $\gamma_{\mathrm{eff}}/2\pi \simeq 97$ Hz. This value is slightly higher than the intrinsic linewidth γ because of a finite negative detuning and consequently some optical damping. Nonetheless, the cooling due to the optical damping is negligible. Finally, in Fig. 3(d), we show the mechanical occupation number that can be reached in our setup. The occupation is calculated with Eq. (16) with use of the calibrated quantities and the bath temperature obtained from our fitting the spectra. We reach an occupation of $n_m = 2.9 \pm 0.3$ quanta, which is significantly close to the ground state, and is limited by the amplifier added noise injected back into the sample.

B. Probing at the blue optomechanical sideband

We next move the probe tone from the cavity center frequency to the blue-optomechanical-sideband frequency. Since the probe tone at its final intended power pushes the oscillator far into the instability regime, the feedback parameters are first optimized at a low probe power, only incrementally reaching higher powers by our exploring small parameter ranges around the stability regime. Figure 4 shows the result of gain sweeps performed at the highest probe power used in this configuration, and at the optimal feedback phase. The investigation of small gains is precluded by instability at low feedback efficiencies.
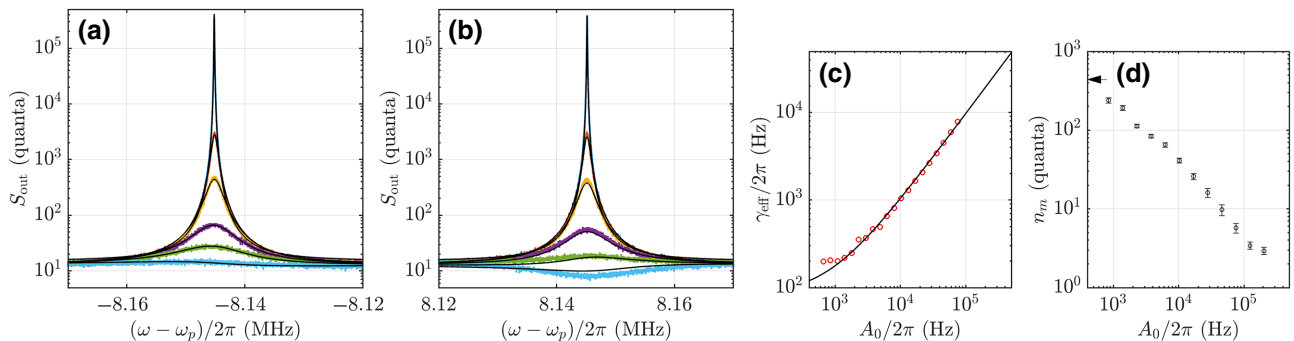

FIG. 3. Feedback cooling. The parameter values are $G/2\pi \simeq 427$ kHz and $\phi \simeq 143°$. (a),(b) In-loop heterodyne output spectra at the lower and upper sideband, respectively. The gain values are $A_0/2\pi \simeq 0, 10, 28, 76, 125$, and 206 kHz from top to bottom. The solid lines are theoretical fits. (c) Damping rate extracted by our fitting Lorentzian curves to the spectra at lower gain values, together with a fit to Eq. (9b). The data are shown in the range where the peaks are roughly Lorentzian. (d) Mechanical occupation as a function of feedback gain. The arrow indicates the value $n_m \simeq 440$ at zero gain.
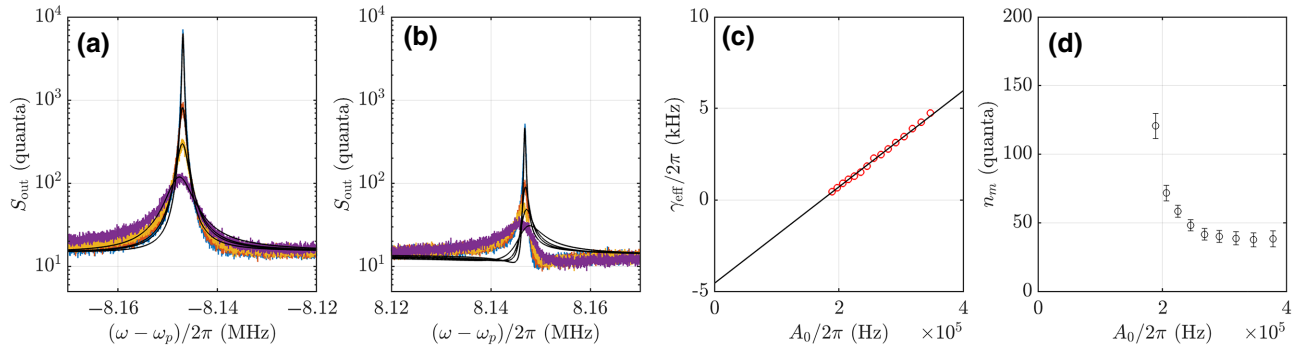
FIG. 4. Feedback stabilization and cooling of an intrinsically unstable system. The probe tone is set at the blue-sideband frequency ($\Delta = \omega_m$), and the effective coupling is $G/2\pi \simeq 104$ kHz. The gain values are $A_0/2\pi \simeq 189$, 225, 267, and 378 kHz from top to bottom. The same quantities are presented as in the resonant-pumping case, Fig. 3. (a),(b) Lower-sideband and upper-sideband peaks around the probe tone, respectively. (c) Effective damping in the stable range. (d) Mechanical occupation as a function of feedback gain.

The lower-sideband peak shown in Fig. 4(a), which in this case is located at the cavity frequency, exhibits good agreement with the numerically computed line shape for each gain displayed as solid black lines. The upper-sideband peak shown in Fig. 4(b) is strongly suppressed by the unfavorable cavity susceptibility as this signal is detuned from the cavity by approximately twice the cavity linewidth. With the upper sideband, we acknowledge a discrepancy between the theoretical line shapes also displayed in Fig. 4(b). We again anticipate some additional noise is circulating in the feedback loop at frequencies near the upper sideband of the probe tone, inducing additional squashing effects. The calibrated height of the peaks, however, matches well with the predictions.

Similarly to the resonant-pumping case, we again use the mechanical-bath temperature as a free parameter in the fits to the line shapes. We consider only the strong, lower sideband in the fitting. Here we find a very strong technical

heating when the feedback gain increases: the mechanical bath heats up to $n_m^T \simeq 5 \times 10^3$ phonons at the maximum gain $A_0/2\pi \simeq 400$ kHz (Fig. 5).

As shown in Fig. 4(c), a sizable damping rate $\gamma_{\text{eff}}/2\pi \simeq 5$ kHz can be obtained in the blue-sideband configuration. This damping is not only significant considering that the oscillator is antidamped at zero gain but is also nearly 2 orders of magnitude larger than the intrinsic damping. Finally, in Fig. 4(d) we display the mechanical occupation inferred in the situation using our numerical model. We obtain a modest cooling down to $n_m \simeq 38$, limited primarily by the technical heating.

V. CONCLUSIONS

In summary, we demonstrate feedback cooling in a microwave optomechanical system. We reach a mechanical occupation $n_m \simeq 3$ quanta in an 8-MHz membrane resonator. The cooling is limited by the added noise of the microwave amplifier. By the introduction of traveling-wave Josephson parametric amplifiers, which exhibit near-quantum-limited-noise performance [40,41] with $n_{\text{add}} \sim$ 1–1.5 quanta, ground-state cooling with the parameters used in this work should be well within reach. This will open up possibilities for feedback-based preparation of more-sophisticated states, such as squeezed states [42], through backaction-evading measurements.
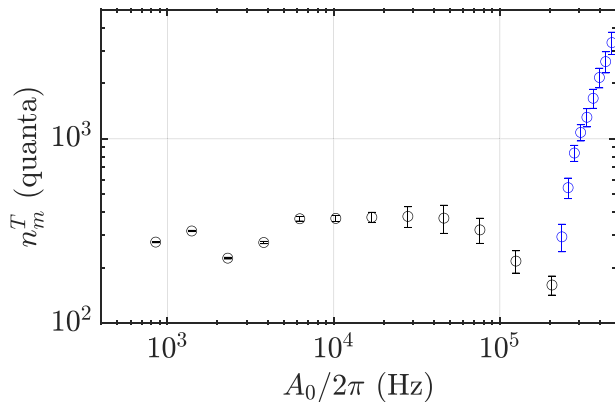
FIG. 5. Technical heating. Bath temperature of the mechanical oscillator as a function of feedback gain. Black circles represent resonant probing, and blue circles represent blue-sideband probing.

APPENDIX A: SOLVING THE CLOSED-LOOP DYNAMICS

In the bad-cavity case there are simple analytical results for the entire system, including the output spectrum due to the probe tone (Appendix B). Also, with arbitrary sideband resolution but restricted to $\Delta = 0$, we can recover expressions for the mechanical occupation, Eq. (16), and the preceding equations. However, with the current parameters we always calculate the output spectrum numerically. We start from Eq. (4), and write the connection of the variables to the inputs with coefficients to be determined:

$$x_c = X_{cx}x_{c,\mathrm{in}}, \tag{A1a}$$

$$y_c = Y_{cy}y_{c,\mathrm{in}} + Y_x x_{c,\mathrm{in}} + Y_f f_{\mathrm{th}} + Y_n y_{\mathrm{add}}, \tag{A1b}$$

$$x = X_f f_{\mathrm{th}} + X_{BAx}x_{c,\mathrm{in}} + X_{\mathrm{inj}}y_{c,\mathrm{in}} + X_n y_{\mathrm{add}}, \tag{A1c}$$

$$p = P_f f_{\mathrm{th}} + P_{BAx}x_{c,\mathrm{in}} + P_{\mathrm{inj}}y_{c,\mathrm{in}} + P_n y_{\mathrm{add}}. \tag{A1d}$$

As an example, the term with X_{BAx} gives the quantum measurement backaction to the position, X_{inj} describes how the quantum noise in the feedback loop is injected back into the sample, and $X_n = X_{\mathrm{inj}}$ is a similar injection of amplifier noise. To continue with the example, in the case $\Delta = 0$,

$$\begin{aligned} X_f &= \chi_{\mathrm{FB}}, \\ X_{\mathrm{inj}} &= -\frac{4G\omega_m\sqrt{\kappa}}{\kappa - 2i\omega}\chi_{\mathrm{FB}}, \end{aligned} \tag{A2}$$

with χ_{FB} given by Eq. (8).

1. Noise considerations

In this section, we assume that the optimal feedback condition is met; that is, $\phi = \phi_m$ [Eq. (10)]. In this case,

$$\begin{aligned} f_{\mathrm{FB}}[\omega] = {} & \frac{i2GA_0}{\sqrt{\kappa^2/4 + \omega_m^2}}x[\omega] \\ & + \frac{A_0\omega_m}{\sqrt{\kappa}}e^{-i\phi\frac{\omega}{\omega_m}}\Big((\kappa\chi_c[\omega] - 1)y_{c,\mathrm{in}}[\omega] + y_{\mathrm{add}}\Big). \end{aligned} \tag{A3}$$

The first term of the feedback force is responsible for feedback damping. The second term accounts for noise coming from the cavity quantum fluctuations reinjected in

the feedback loop, as well as added noise from the detection stage (mainly amplifier added noise), also fed back to the oscillator. As a result, the position satisfies the equation

$$\begin{aligned} x = \chi_{\mathrm{FB}}\Big[& f_{\mathrm{th}} - 2\omega_m G x_c \\ & + \frac{A_0\omega_m}{\sqrt{\kappa}}e^{-i\phi\frac{\omega}{\omega_m}}\Big((\kappa\chi_c - 1)y_{c,\mathrm{in}} + y_{\mathrm{add}}\Big)\Big], \end{aligned} \tag{A4}$$

with $x_c = \chi_c\sqrt{\kappa}x_{c,\mathrm{in}}$. In Eq. A4, the first term accounts for thermal noise, the second accounts for measurement-backaction noise, and the third accounts for the total measurement noise fed back to the oscillator, which is the sum of the two contributions discussed above. All noise processes appearing in these equations are uncorrelated, so the contributions do not interfere. Assuming (as always) that $\gamma \ll \kappa$ and that the cavity is in its ground state, the backaction noise arising from the second term in Eq. (A4) gives Eq. (13). The third term in Eq. (A4) leads to the total measurement noise fed back to the oscillator, Eq. (15).

APPENDIX B: SPECTRUM IN THE UNRESOLVED-SIDEBAND SITUATION

The "noise squashing" in the bad-cavity situation allows simple analytical results to be obtained. At the optimum feedback phase in this situation, $\phi_m = \pi/2$, the in-loop heterodyne spectrum can be understood as consisting of two Lorentzians with opposite signs:

$$\begin{aligned} S_{\mathrm{out},x}[\omega] &= \frac{8G^2}{\kappa}S_x[\omega], \\ S_{\mathrm{out},\pm}[\omega] &= -\frac{GA_0\omega_m\gamma_{\mathrm{eff}}/\kappa(n_{\mathrm{add}} + \frac{1}{2})}{(\omega \mp \omega_m)^2 + (\frac{\gamma_{\mathrm{eff}}}{2})^2}, \end{aligned} \tag{B1}$$

and $S_{\mathrm{out}}[\omega] = S_{\mathrm{out},x}[\omega] + S_{\mathrm{out},-}[\omega] + S_{\mathrm{out},+}[\omega] + n_{\mathrm{add}} + \frac{1}{2}$. The term $S_{\mathrm{out},x}[\omega]$ gives the sideband asymmetry, while the squashing term is the same for the lower sideband and the upper sideband.

In the case of weak feedback, $S_{\mathrm{out},+}$ and $S_{\mathrm{out},-}$ are negligible.

APPENDIX C: ELECTROMECHANICAL FORCES

The intracavity field-annihilation operator can be decomposed into $a = \alpha(t) + \alpha_f(t) + \tilde{a}(t)$, where $\tilde{a}$ is a (quantum) annihilation operator associated with a small fluctuation, α is the classical complex amplitude of the probe tone oscillating at ω_c or $\omega_c + \omega_m$, and α_f is the classical complex amplitude of the feedback tone oscillating at $\omega_c + \Delta_f \pm \omega_m$. Notice the above does not yet imply linearization of the optomechanical interaction. The evolution

equation for the mechanical-oscillator momentum is

$$\dot{p} = -\gamma p - \omega_m x - \sqrt{2}g_0 a^\dagger a + \frac{f_{\text{th}}}{\omega_m}. \qquad \text{(C1)}$$

The total electromechanical force $-\sqrt{2}g_0 a^\dagger a$ contains the following terms:

(a) $-\sqrt{2}g_0|\alpha_f|^2$: feedback force
(b) $-\sqrt{2}g_0|\alpha|^2$: a dc force from the probe tone
(c) $-\sqrt{2}g_0(\alpha\tilde{a}^\dagger + \alpha^*\tilde{a})$: dynamical and quantum back-action from the probe tone
(d) $-\sqrt{2}g_0(\alpha_f\tilde{a}^\dagger + \alpha_f^*\tilde{a})$: dynamical and quantum back-action from the feedback tone

The force also contains cross-products of the probe and feedback tones (oscillating at Δ_f or $\Delta_f + \omega_m$) that are largely out of resonance with the mechanical oscillator and whose impact is ignored. Finally, it also contains terms such as $-2g_0\tilde{a}^\dagger\tilde{a}$ coming from quantum fluctuations of the cavity field, which is, as usual in driven-cavity optomechanics, ignored compared with all other forces as it is typically much weaker.

1. Probe tone at the cavity center frequency

We now derive α_f to give the expression for the feedback force in the situation where the probe tone is sent at the cavity center frequency. The position signal in frequency space is

$$x[\omega] \equiv \frac{b[\omega] + b^\dagger[\omega]}{\sqrt{2}}, \qquad \text{(C2)}$$

with b ($b^\dagger$) the annihilation (creation) operator in the laboratory frame. In the following, we also use phase-shifted position signals

$$x_\varphi[\omega] \equiv \frac{b[\omega]e^{i\varphi} + b^\dagger[\omega]e^{-i\varphi}}{\sqrt{2}}. \qquad \text{(C3)}$$

The inverse Fourier transform of x_φ is, in the limit of small delays compared with the decoherence time, the delayed position signal $x_\varphi(t) \simeq x(t - \varphi/\omega_m)$. In the following subsection, we assume the small-delay condition is systematically satisfied. The cavity quadrature coupled to the motion is given by

$$y_c[\omega] = \chi_c[\omega]\left[-\sqrt{2}G\left(b[\omega] + b^\dagger[\omega]\right) + \sqrt{\kappa}\, y_{c,\,\text{in}}[\omega]\right]. \qquad \text{(C4)}$$

Each operator (b, $b^\dagger$) selects a narrow frequency range ($+\omega_m$, $-\omega_m$) over which the cavity susceptibility can be considered constant. That is, $b[\omega]$ and $b^\dagger[\omega]$ sample

the cavity susceptibility at different (opposite) frequencies $\pm\omega_m$, such that

$$y_c[\omega] \simeq -\sqrt{2}G|\chi_c[\omega_m]|\left(b[\omega]e^{i\phi_0} + b^\dagger[\omega]e^{-i\phi_0}\right),$$
$$+ \chi_c[\omega]\sqrt{\kappa}\, y_{c,\,\text{in}}[\omega], \qquad \text{(C5)}$$

where

$$\phi_0 \equiv \arg\{\chi_c[\omega_m]\} = \arctan\left(\frac{2\omega_m}{\kappa}\right)$$

$$|\chi_c[\omega_m]| \equiv (\kappa^2/4 + \omega_m^2)^{-1/2}. \qquad \text{(C6)}$$

If we ignore cavity noise, the corresponding output quadrature is given by

$$y_{\text{out}}[\omega] = \sqrt{\kappa}y_c[\omega] - y_{c,\,\text{in}}[\omega]$$
$$= \frac{2\sqrt{\kappa}G}{\sqrt{\kappa^2/4 + \omega_m^2}}\, x_{\phi_0}[\omega] + (\kappa\chi_c[\omega] - 1)\, y_{c,\,\text{in}}[\omega]. \qquad \text{(C7)}$$

We ignore cavity noise in the following. The feedback loop applies a filter that amplifies this signal by a gain $\mathcal{G}$ and delays it by τ. The equivalent phase shift for an oscillator at ω_m is $\phi_\tau \equiv \omega_m\tau$. The unit of $\mathcal{G}$ is chosen such that the result of the filtering operation is a dimensionless signal $s(t)$ whose Fourier transform is given by

$$s[\omega] = \frac{2\mathcal{G}\sqrt{\kappa}G}{\sqrt{\kappa^2/4 + \omega_m^2}}\, x_{\phi_0+\phi_\tau}[\omega]. \qquad \text{(C8)}$$

This signal is sent to a phase modulator driven by a coherent pump at ω_f and of amplitude α_0/π. The result of this modulation is an electronic signal

$$\alpha_{f,\text{mod}}(t) = \alpha_0/\pi \, \sin(\omega_f t + s(t)). \qquad \text{(C9)}$$

In the equation above, the conversion factor affecting $s(t)$ in the mixing operation is also integrated into $\mathcal{G}$, and therefore $s(t)$, for convenience. Finally, if $|s(t)| \ll 2\pi$, if we use $\sin s(t) \simeq s(t)$ and $\cos s(t) \simeq 1$, this signal corresponds to the sum of a strong coherent tone oscillating at ω_f and a weaker signal at ω_f whose amplitude is modulated by $s(t)$:

$$\alpha_{f,\text{mod}}(t) \simeq \alpha_0/\pi \left(\sin \omega_f t + s(t) \cos \omega_f t \right). \qquad \text{(C10)}$$

The corresponding complex amplitude in the frame oscillating at the cavity resonance frequency is given by

$$\alpha_{f,\text{in}}[\omega] = i\alpha_0\delta(\omega - \Delta_f) + \frac{\alpha_0\mathcal{G}\sqrt{\kappa}2G}{\sqrt{\kappa^2/4 + \omega_m^2}}\, x_{\phi_0+\phi_\tau}[\omega - \Delta_f]. \qquad \text{(C11)}$$

This signal is driving the cavity to apply the feedback force. The spectrum of this signal is a triplet of peaks:

one strong peak of amplitude α_0 at $\omega = \omega_c + \Delta_f$ and two weaker sidebands (weak as per the assumption above, $|s(t)| \ll 2\pi$), whose spectrum reproduces the spectrum of x, oscillating at frequencies $\omega = \omega_c + \Delta_f \pm \omega_m$. Since these three peaks sit at significantly different frequencies compared with the cavity linewidth, they are affected differently by the cavity susceptibility. In particular, they will be affected by different phase shifts due to the cavity susceptibility denoted ϕ_1, ϕ_+, and ϕ_-.

$$\alpha_f[\omega] = \frac{\alpha_0 \mathcal{G} \kappa \sqrt{2} G}{\sqrt{\kappa^2/4 + \omega_m^2}} \left(\frac{b[\omega - \Delta_f]e^{i(\phi_0 + \phi_\tau + \phi_+)}}{\sqrt{\kappa^2/4 + (\Delta_f + \omega_m)^2}} \right.$$
$$+ \frac{b^\dagger[\omega - \Delta_f]e^{-i(\phi_0 + \phi_\tau - \phi_-)}}{\sqrt{\kappa^2/4 + (\Delta_f - \omega_m)^2}} \left. \right)$$
$$+ \alpha_0 \sqrt{\kappa} \frac{\delta(\omega - \Delta_f)e^{i(\phi_1 + \pi/2)}}{\sqrt{\kappa^2/4 + \Delta_f^2}}, \qquad \text{(C12)}$$

with

$$\phi_1 = \tan^{-1} \frac{2\Delta_f}{\kappa},$$
$$\phi_+ = \tan^{-1} \frac{2(\Delta_f + \omega_m)}{\kappa}, \text{ and } \phi_- = \tan^{-1} \frac{2(\Delta_f - \omega_m)}{\kappa}. \qquad \text{(C13)}$$

a. Feedback force

The linear feedback force therefore comes from a cross-product of either sideband of the drive with the central peak of the drive (if we ignore the added noise contribution for now):

$$f_{\text{FB}}[\omega] = -g_0 \frac{\kappa^{3/2} \alpha_0^2 \mathcal{G} 2G}{\sqrt{(\kappa^2/4 + \omega_m^2)(\kappa^2/4 + \Delta_f^2)}}$$
$$\left(\frac{x_{\phi_0 + \phi_\tau + \phi_+ - \phi_1 - \pi/2}[\omega]}{\sqrt{\kappa^2/4 + (\Delta_f + \omega_m)^2}} \right.$$
$$+ \left. \frac{x_{\phi_0 + \phi_\tau - \phi_- + \phi_1 + \pi/2}[\omega]}{\sqrt{\kappa^2/4 + (\Delta_f - \omega_m)^2}} \right). \qquad \text{(C14)}$$

The force therefore has two contributions. This results from each of the sidebands of the driving triplet interfering with the central peak to give a force contribution. Each of these forces contains a phase-shifted version of the position, with a different phase shift for each, due to the frequency dependence of the cavity-susceptibility phase. In the limit of small delays compared with the decoherence rate, the sum of the two position signals with different phase shifts is itself a phase-shifted position signal. If we denote the phase shifts as $\varphi = \phi_\tau + \phi_+ - \phi_1 - \pi/2$ and $\varphi' = \phi_\tau - \phi_- + \phi_1 + \pi/2$ and the coefficients $A = \kappa/\sqrt{\kappa^2/4 + (\Delta_f + \omega_m)^2}$ and $B =$

$\kappa/\sqrt{\kappa^2/4 + (\Delta_f - \omega_m)^2}$, the force is then written as (again if we ignore the noise contribution)

$$f_{\text{FB}}[\omega] = -\frac{2G}{\sqrt{\kappa^2/4 + \omega_m^2}} \frac{g_0 \sqrt{\kappa} \alpha_0^2 \mathcal{G}}{\sqrt{\kappa^2/4 + \Delta_f^2}} D x_{\phi_0 + \phi}[\omega], \qquad \text{(C15)}$$

with $D \equiv \sqrt{A^2 + B^2 + 2AB \cos(\varphi - \varphi')}$ and $\phi \equiv \arctan(A \sin \varphi + B \sin \varphi')/(A \cos \varphi + B \cos \varphi')$. We can now identify the phase shift ϕ of the feedback filtering application as defined in the main text, as well as the gain A_0,

$$A_0 = \frac{g_0 \sqrt{\kappa} \alpha_0^2 \mathcal{G}}{\sqrt{\kappa^2/4 + \Delta_f^2}} D, \qquad \text{(C16)}$$

which is proportional to $\mathcal{G}$. We also see that because the two position signals contributing to the feedback force are not affected by the same phase shift, their sum is only partially constructive. Indeed, the gain A_0 is maximum when φ and φ' are equal. On the other hand, if one force contribution largely dominates over the other, then the interference between these two contributions is weak. The only very unfavorable situation, which makes A_0 vanish, is therefore the bad-cavity limit, wherein the amplitudes of the two contributions are similar and $\varphi - \varphi' \simeq -\pi$. In the experimental situation, not accounting for phase shifts incurred in the propagation in transmission lines, the phase difference between force components $\varphi - \varphi' = \phi_+ + \phi_- - 2\phi_1 - \pi$ is about $-176°$, which would be quite unfavorable. However, the sideband at $\omega_c + \omega_m + \Delta_f$ of the feedback triplet is more than twice as strong as the sideband at $\omega_c - \omega_m + \Delta_f$, limiting the destructive interference's impact. Furthermore, as they come from signals at different frequencies, φ and φ' are also impacted by different phase shifts accumulated in the propagation in transmission lines, which are not accounted for in the latter estimate. In conclusion, even in the worst phase configuration, where the two feedback-force contributions interfere destructively, the fact that one dominates over the other ensures that the destructive interference is not complete and that the feedback force is significant.

APPENDIX D: DATA ANALYSIS

The effective coupling G at a given generator power is obtained on the basis of a standard power sweep in a sideband-cooling measurement, where the pump frequency is set at the red sideband. The optomechanical damping is fitted linearly with the generator power P:

$$\gamma_{\text{opt}} = \mathcal{P} P, \qquad \text{(D1)}$$

where $\mathcal{P}$ is the calibration coefficient. The effective coupling under the red-sideband probing is obtained from

Eq. (19) as

$$G_{\text{RSB}} = \frac{1}{2}\sqrt{\mathcal{P}P\kappa\left[1 + \left(\frac{\kappa}{4\omega_m}\right)^2\right]}. \qquad \text{(D2)}$$

In determining G in the feedback experiment, we have to account for the specific probe-tone detuning because the field amplitude in the cavity, at a given generator power, depends on the cavity susceptibility:

$$G = \frac{|\chi_c(\Delta)|}{|\chi_c(-\omega_m)|}G_{\text{RSB}}, \qquad \text{(D3)}$$

where Δ is the specific detuning, which can be either 0 or ω_m.

The gain A_0 used in the theoretical discussion is not a quantity directly applicable to the experiment. The experimentally relevant gain $\mathcal{G}$ is simply proportional to it, with an unknown coefficient coming from the transduction.

The values of A_0 calibrated as described immediately below are used when we are fitting the theoretically obtained output spectrum to the feedback data, and to infer the mechanical occupation.

1. Resonant probing

We fit the measured linewidths as follows to obtain the calibration coefficient $\mathcal{L}$:

$$\gamma_{\text{FB}} = \mathcal{L}\mathcal{G}. \qquad \text{(D4)}$$

We combine Eq. (D4) with Eq. (11):

$$A_0 = \frac{\mathcal{L}\mathcal{G}\sqrt{\kappa^2 + 4\omega_m^2}}{4G}. \qquad \text{(D5)}$$

2. Blue-sideband probing

Here we use the damping stated in Eq. (20), and obtain at the optimum phase

$$\gamma_{\text{eff}} = \gamma - \gamma_{\text{opt}} + \gamma_{\text{FB,BSB}}, \qquad \text{(D6)}$$

where

$$\gamma_{\text{FB,BSB}} = \frac{4A_0 G\sqrt{\kappa^4 + 20\kappa^2\omega_m^2 + 64\omega_m^4}}{\kappa^3 + 16\kappa\omega_m^2}. \qquad \text{(D7)}$$

We fit to Eqs. (D6) and (D7) the measured linewidth with increasing gain, in a manner similar to that described in Eq. (D5) for the resonant-probing situation.

3. Error analysis

As mentioned in the main text, the occupation numbers under feedback cooling are calculated from Eq. (16). To evaluate the error bars of these quantities, we propagate 2σ uncertainties in this equation. The quantities that have significant uncertainties are the bath temperature n_m^T and A_0. The error bars of n_m^T are the statistical errors from the fit to the full theoretical model. For A_0, a significant uncertainty comes from the calibration coefficient $\mathcal{L}$ in Eq. (D4).

---

[1] P. F. Cohadon, A. Heidmann, and M. Pinard, Cooling of a Mirror by Radiation Pressure, Phys. Rev. Lett. **83**, 3174 (1999).

[2] Dustin Kleckner and Dirk Bouwmeester, Sub-kelvin optical cooling of a micromechanical resonator, Nature **444**, 75 (2006).

[3] M. Poggio, C. L. Degen, H. J. Mamin, and D. Rugar, Feedback Cooling of a Cantilever's Fundamental Mode below 5 mK, Phys. Rev. Lett. **99**, 017201 (2007).

[4] A. Vinante, M. Bignotto, M. Bonaldi, M. Cerdonio, L. Conti, P. Falferi, N. Liguori, S. Longo, R. Mezzena, A. Ortolan, G. A. Prodi, F. Salemi, L. Taffarello, G. Vedovato, S. Vitale, and J.-P. Zendri, Feedback Cooling of the Normal Modes of a Massive Electromechanical System to Submillikelvin Temperature, Phys. Rev. Lett. **101**, 033601 (2008).

[5] D. J. Wilson, V. Sudhir, N. Piro, R. Schilling, A. Ghadimi, and T. J. Kippenberg, Measurement-based control of a mechanical oscillator at its thermal decoherence rate, Nature **524**, 325 (2015).

[6] Clemens Schäfermeier, Hugo Kerdoncuff, Ulrich B. Hoff, Hao Fu Alexander Huck, Jan Bilek, Glen I. Harris, Warwick P. Bowen, Tobias Gehring, and Ulrik L. Andersen, Quantum enhanced feedback cooling of a mechanical oscillator using nonclassical light, Nat. Commun. **7**, 13628 (2016).

[7] Massimiliano Rossi, Nenad Kralj, Stefano Zippilli, Riccardo Natali, Antonio Borrielli, Gregory Pandraud, Enrico Serra, Giovanni Di Giuseppe, and David Vitali, Enhancing Sideband Cooling by Feedback-Controlled Light, Phys. Rev. Lett. **119**, 123603 (2017).

[8] V. Sudhir, D. J. Wilson, R. Schilling, H. Schütz, S. A. Fedorov, A. H. Ghadimi, A. Nunnenkamp, and T. J. Kippenberg, Appearance and Disappearance of Quantum Correlations in Measurement-Based Feedback Control of a Mechanical Oscillator, Phys. Rev. X **7**, 011001 (2017).

[9] Philipp Christoph, Tobias Wagner, Hai Zhong, Roland Wiesendanger, Klaus Sengstock, Alexander Schwarz, and Christoph Becker, Combined feedback and sympathetic cooling of a mechanical oscillator coupled to ultracold atoms, New J. Phys. **20**, 093020 (2018).

[10] Jingkun Guo, Richard Norte, and Simon Gröblacher, Feedback Cooling of a Room Temperature Mechanical Oscillator Close to Its Motional Ground State, Phys. Rev. Lett. **123**, 223602 (2019).

[11] Arvind Shankar Kumar, Joonas Nätkinniemi, Henri Lyyra, and Juha T. Muhonen, Single-laser feedback cooling of optomechanical resonators, (2022), ArXiv:2209.06029.

[12] Massimiliano Rossi, David Mason, Junxin Chen, Yeghishe Tsaturyan, and Albert Schliesser, Measurement-based quantum control of mechanical motion, Nature **563**, 53 (2018).

[13] B. Abbott, R. Abbott, R. Adhikari, P. Ajith, B. Allen, G. Allen, R. Amin, S. B. Anderson, W. G. Anderson, M. A. Arain, and M. Araya, Observation of a kilogram-scale oscillator near its quantum ground state, New J. Phys. **11**, 073032 (2009).

[14] C. Whittle, E. D. Hall, S. Dwyer, N. Mavalvala, V. Sudhir, R. Abbott, A. Ananyeva, C. Austin, L. Barsotti, J. Betzwieser, and C. D. Blair, Approaching the motional ground state of a 10-kg object, Science **372**, 1333 (2021).

[15] Jan Gieseler, Bradley Deutsch, Romain Quidant, and Lukas Novotny, Subkelvin Parametric Feedback Cooling of a Laser-Trapped Nanoparticle, Phys. Rev. Lett. **109**, 103603 (2012).

[16] Jamie Vovrosh, Muddassar Rashid, David Hempston, James Bateman, Mauro Paternostro, and Hendrik Ulbricht, Parametric feedback cooling of levitated optomechanics in a parabolic mirror trap, J. Opt. Soc. Am. B **34**, 1421 (2017).

[17] Tongcang Li, Simon Kheifets, and Mark G. Raizen, Millikelvin cooling of an optically trapped microsphere in vacuum, Nat. Phys. **7**, 527 (2011).

[18] Gerard P. Conangla, Francesco Ricci, Marc T. Cuairan, Andreas W. Schell, Nadine Meyer, and Romain Quidant, Optimal Feedback Cooling of a Charged Levitated Nanoparticle with Adaptive Control, Phys. Rev. Lett. **122**, 223602 (2019).

[19] M. Iwasaki, T. Yotsuya, T. Naruki, Y. Matsuda, M. Yoneda, and K. Aikawa, Electric feedback cooling of single charged nanoparticles in an optical trap, Phys. Rev. A **99**, 051401(R) (2019).

[20] Uroš Delić, Manuel Reisenbauer, Kahan Dare, David Grass, Vladan Vuletić, Nikolai Kiesel, and Markus Aspelmeyer, Cooling of a levitated nanoparticle to the motional quantum ground state, Science **367**, 892 (2020).

[21] Felix Tebbenjohanns, M. Luisa Mattana, Massimiliano Rossi, Martin Frimmer, and Lukas Novotny, Quantum control of a nanoparticle optically levitated in cryogenic free space, Nature **595**, 378 (2021).

[22] C. A. Regal, J. D. Teufel, and K. W. Lehnert, Measuring nanomechanical motion with a microwave cavity interferometer, Nat. Phys. **4**, 555 (2008).

[23] J. D. Teufel, T. Donner, Dale Li, J. W. Harlow, M. S. Allman, K. Cicak, A. J. Sirois, J. D. Whittaker, K. W. Lehnert, and R. W. Simmonds, Sideband cooling of micromechanical motion to the quantum ground state, Nature **475**, 359 (2011).

[24] Stefano Mancini, David Vitali, and Paolo Tombesi, Optomechanical Cooling of a Macroscopic Oscillator by Homodyne Feedback, Phys. Rev. Lett. **80**, 688 (1998).

[25] David Vitali, Stefano Mancini, Luciano Ribichini, and Paolo Tombesi, Mirror quiescence and high-sensitivity position measurements with feedback, Phys. Rev. A **65**, 063803 (2002).

[26] Asa Hopkins, Kurt Jacobs, Salman Habib, and Keith Schwab, Feedback cooling of a nanomechanical resonator, Phys. Rev. B **68**, 235328 (2003).

[27] C. Genes, D. Vitali, P. Tombesi, S. Gigan, and M. Aspelmeyer, Ground-state cooling of a micromechanical oscillator: Comparing cold damping and cavity-assisted cooling schemes, Phys. Rev. A **77**, 033804 (2008).

[28] Jing Zhang, Yu xi Liu, Re-Bing Wu, Kurt Jacobs, and Franco Nori, Quantum feedback: Theory, experiments, and applications, Phys. Rep. **679**, 1 (2017).

[29] Christian Sommer and Claudiu Genes, Partial Optomechanical Refrigeration via Multimode Cold-Damping Feedback, Phys. Rev. Lett. **123**, 203605 (2019).

[30] M. J. Woolley and A. A. Clerk, Two-mode back-action-evading measurements in cavity optomechanics, Phys. Rev. A **87**, 063846 (2013).

[31] E. E. Wollman, C. U. Lei, A. J. Weinstein, J. Suh, A. Kronwald, F. Marquardt, A. A. Clerk, and K. C. Schwab, Quantum squeezing of motion in a mechanical resonator, Science **349**, 952 (2015).

[32] F. Lecocq, J. B. Clark, R. W. Simmonds, J. Aumentado, and J. D. Teufel, Quantum Nondemolition Measurement of a Nonclassical State of a Massive Object, Phys. Rev. X **5**, 041037 (2015).

[33] J.-M. Pirkkalainen, E. Damskägg, M. Brandt, F. Massel, and M. A. Sillanpää, Squeezing of Quantum Noise of Motion in a Micromechanical Resonator, Phys. Rev. Lett. **115**, 243601 (2015).

[34] C. F. Ockeloen-Korppi, E. Damskägg, J. M. Pirkkalainen, M. Asjad, A. A. Clerk, F. Massel, M. J. Woolley, and M. A. Sillanpää, Stabilized entanglement of massive mechanical oscillators, Nature **556**, 478 (2018).

[35] X. Zhou, D. Cattiaux, R. R. Gazizulin, A. Luck, O. Maillet, T. Crozes, J.-F. Motte, O. Bourgeois, A. Fefferman, and E. Collin, On-Chip Thermometry for Microwave Optomechanics Implemented in a Nuclear Demagnetization Cryostat, Phys. Rev. Appl. **12**, 044066 (2019).

[36] Leonhard Neuhaus and Samuel Deléglise, *et al.*, PyRPL open-source software: https://pyrpl.readthedocs.io/en/latest/index.html.

[37] A. J. Weinstein, C. U. Lei, E. E. Wollman, J. Suh, A. Metelmann, A. A. Clerk, and K. C. Schwab, Observation and Interpretation of Motional Sideband Asymmetry in a Quantum Electromechanical Device, Phys. Rev. X **4**, 041003 (2014).

[38] M. Underwood, D. Mason, D. Lee, H. Xu, L. Jiang, A. B. Shkarin, K. Børkje, S. M. Girvin, and J. G. E. Harris, Measurement of the motional sidebands of a nanogram-scale oscillator in the quantum regime, Phys. Rev. A **92**, 061801(R) (2015).

[39] F. Lecocq, J. D. Teufel, J. Aumentado, and R. W. Simmonds, Resolving the vacuum fluctuations of an optomechanical system using an artificial atom, Nat. Phys. **11**, 635 (2015).

[40] C. Macklin, K. O'Brien, D. Hover, M. E. Schwartz, V. Bolkhovsky, X. Zhang, W. D. Oliver, and I. Siddiqi, A near-quantum-limited Josephson traveling-wave parametric amplifier, Science **350**, 307 (2015).

[41] M. R. Perelshtein, K. V. Petrovnin, V. Vesterinen, S. Hamedani Raja, I. Lilja, M. Will, A. Savin, S. Simbierow-icz, R. N. Jabdaraghi, J. S. Lehtinen, L. Grönberg, J. Hassel, M. P. Prunnila, J. Govenius, G. S. Paraoanu, and P. J. Hako-nen, Broadband Continuous-Variable Entanglement Gen-eration Using a Kerr-Free Josephson Metamaterial, Phys. Rev. Appl. **18,** 024063 (2022).

[42] A. A. Clerk, F. Marquardt, and K. Jacobs, Back-action eva-sion and squeezing of a mechanical resonator using a cavity detector, New J. Phys. **10,** 095010 (2008).